Appl. Phys. B 30, 87–94 (1983)

Applied Physics B Photophysics and Laser Chemistry

Diffraction Efficiencies of Evanescent-Wave Holograms

An Improved Model

W. Biehlig, U. Langbein, and F. Lederer

Department of Physics, University of Jena, DDR-69 Jena, German Democratic Republic

Received 1 July 1982/Accepted 1 October 1982

Abstract. In contrast to previous models diffraction efficiencies of evanescent-wave holograms are calculated within the framework of a slab model that takes into account the finite thickness of the recording medium. This modification leads to characteristic diffraction efficiency oscillations with respect to reconstruction angle and medium thickness as well. One obtains higher diffraction efficiency maxima and pseudo-optical tunnelling. The analysis covers TE-polarized fields.

PACS: 42.40, 42.80

The interference of the evanescent tail of a totally reflected reference wave with an arbitrary object wave provides an intensity pattern which is called evanescent-wave hologram (EWH) after having been recorded in a fotosensitive medium. The intrinsic properties of EWH's (see, for instance, [1–6]) are due to their specific grating patterns which are confined to the immediate vicinity of that boundary of the recording medium where total reflection took place. Two of these properties are: (i) the elegant way of image field separation from the strong unwanted zeroth diffraction order well suited to large aperture processing [8], by total reflection [3], and (ii) their compatibility with integrated-optics implementations. On the other hand, EWH's are useful to study the process of recording and retrieval of evanescent object waves in order to cross the wavelength-resolution limit [11] and to investigate the properties of waveguide holograms at least in a first step [7]. An interesting EWH implementation is the matrix storage device [8].

Due to their thin modulated region along the boundary, diffraction efficiency (DE) is a critical parameter for EWH's. Several models have already been published [3–6], determining DE without full consideration of the slab geometry and using the first Born approximation effectively. In contrast to those models, the aim of this contribution is to take into account the effect of finite hologram thickness (which is the thickness of the whole recording medium) during hologram reconstruction. By introducing a second sharp hologram interface (slab model) we are able to consider interference effects like those observed in [4] which are due to multiple reflections of the reconstruction wave and reconstructed field as well, and its superposition with scattering effects by the evanescent grating. Multiple reflections give rise to repeated interactions with the hologram pattern and should therefore enhance total DE. Additionally a medium "behind" the hologram of suitable high refractive index permits the formation of a homogeneously transmitted reconstructed wave even in the case of an evanescent scattered field inside the hologram ("pseudo-optical tunnelling").

In the first section we derive an integral equation describing the reconstruction process and the appropriate Green's function. At this stage we discuss the approximations made in [3, 5]. Having solved the integral equation in the first Born approximation we compare our numerical results with those predicted by Lee and Streifer [5], and with some experimental investigations [4]. The main consequences of our model are (i) strong oscillations of the angular selectivity and of the thickness dependence curves due to multiple wave interference, (ii) higher DE maxima, (iii) change of the peak shapes and (iv) pseudo-optical tunnelling.

0721-7269/83/0030/0087/$01.60

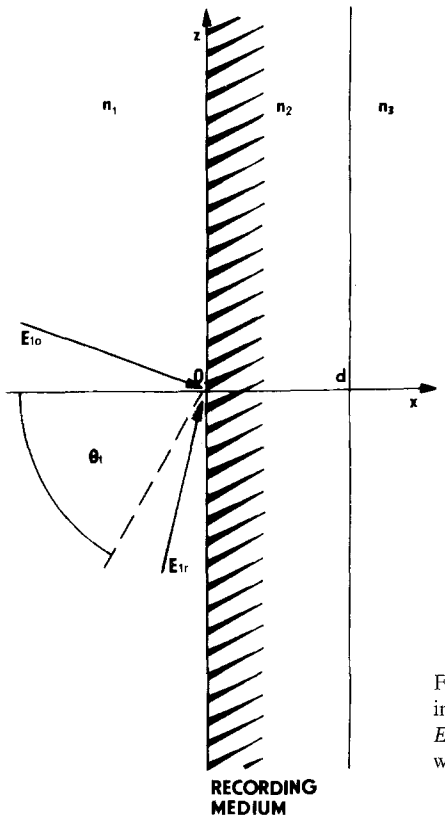

Fig. 1. Hologram recording geometry (θ_t: critical angle of total reflection; n_1, n_2, n_3: refractive indices (n_2: recording medium before exposure; n_1, n_3: surrounding media); E_{1o}: object wave; E_{1r}: reference wave; d: slab thickness). The hatched area indicates the interference pattern within the recording medium

1. Recording and Reconstruction of the Evanescent-Wave Hologram

Assuming translation invariance with respect to the y-direction (Fig. 1) we consider TE polarization only. The time dependence $\exp(-i\omega t)$ is supposed throughout the paper. Just like in [3, 5] the real dielectric function $\varepsilon(x, z)$ characterizing the hologram pattern is assumed as

$$\varepsilon(x,z)=n_2^2+\Delta(n_2^2)+2K\Delta(n_2^2)\exp(-\alpha_{2r}x)\cos[(\beta_0-\beta_r)z+\gamma_{20}x], \tag{1a}$$

$$\varepsilon(x,z)=n_2^2+\Delta(n_2^2)+2K\Delta(n_2^2)\exp[-(\alpha_{20}+\alpha_{2r})x]\cos[(\beta_0-\beta_r)z], \tag{1b}$$

representing slanted (1a) or unslanted (1b) attenuated phase gratings. These gratings give the recorded interference pattern of a homogeneous (1a) or an evanescent (1b) object wave

$$E_{20}(x,z)=A_0\exp[i(\beta_0 z+\gamma_{20}x)], \qquad 0\leqq x\leqq d,$$

$$E_{20}(x,z)=A_0\exp(-\alpha_{20}x)\exp(i\beta_0 z),$$

(the index "2" refers to the slab region, see Fig. 1) with an evanescent reference wave

$$E_{2r}(x,z)=A_r\exp(-\alpha_{2r}x)\exp(i\beta_r z),$$

where reflections at the boundary $x=d$ and the spatial variation of $\Delta(n_2^2)$ have been suppressed.
The following abbreviations were used

$$\gamma_{20}=(k^2n_2^2-\beta_0^2)^{1/2}, \quad \alpha_{20}=(\beta_0^2-k^2n_2^2)^{1/2},$$

$$\gamma_{2r}=(k^2n_2^2-\beta_r^2)^{1/2}, \quad \alpha_{2r}=(\beta_r^2-k^2n_2^2)^{1/2},$$

$k=2\pi/\lambda$, $K=A_r/A_0$, λ: vacuum wavelength.

Figure 2 shows the geometry of the reconstruction process. We consider an incident reconstruction wave

$$E_{1c}(x,z)=A_c\exp[i(\beta_c z+\gamma_{1c}x)], \quad x\leqq 0, \tag{2}$$

$$\gamma_{1c}=(k^2n_1^2-\beta_c^2)^{1/2},$$

whose scattering by the hologram is to be described.

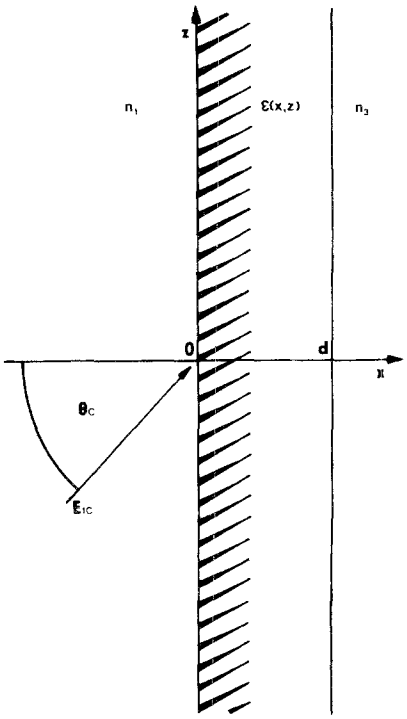

Fig. 2. Hologram reconstruction geometry (θ_c: incidence angle of the reconstruction wave; $\varepsilon(x,z)$: hologram pattern; E_{1c}: reconstruction wave)

Instead of solving Maxwell's equations we prefer the equivalent integral equation approach [9]

$$E(x,z)=E_{\text{hom}}(x,z)+k^2\int_{-\infty}^{\infty}\int_{0}^{d}[\varepsilon(x',z')-n_2'^2]E(x',z')G(x,x';z-z')dx'dz',\ n_2'^2=n_2^2+\Delta(n_2^2), \tag{3}$$

where $E(x,z)$ stands for the resulting total field. $E_{\text{hom}}(x,z)$ denotes the homogeneous solution. It is that field which would exist for vanishing grating modulation $[\varepsilon(x,z)-n_2'^2=0]$. Consequently it satisfies

$$\begin{aligned}
&(\partial^2/\partial x^2+\partial^2/\partial z^2+k^2n_1^2)E_{\text{hom}}(x,z)=0, \quad && x\leqq 0,\\
&(\partial^2/\partial x^2+\partial^2/\partial z^2+k^2n_2'^2)E_{\text{hom}}(x,z)=0, \quad && 0<x<d,\\
&(\partial^2/\partial x^2+\partial^2/\partial z^2+k^2n_3^2)E_{\text{hom}}(x,z)=0, \quad && x\geqq d,
\end{aligned} \tag{4}$$

and together with the corresponding continuity requirement across the slab boundaries we get

$$E_{\text{hom}}(x,z)=A_c\exp(\mathrm{i}\beta_c z)\begin{cases}\exp(\mathrm{i}\gamma_{1c}x)+R\exp(-\mathrm{i}\gamma_{1c}x), & x\leqq 0,\\ 2\gamma_{1c}\dfrac{\gamma_{2c}\cos[\gamma_{2c}(d-x)]-\mathrm{i}\gamma_{3c}\sin[\gamma_{2c}(d-x)]}{\gamma_{2c}(\gamma_{1c}+\gamma_{3c})\cos(\gamma_{2c}d)-\mathrm{i}(\gamma_{2c}^2+\gamma_{1c}\gamma_{3c})\sin(\gamma_{2c}d)}, & 0<x<d,\\ T\exp(\mathrm{i}\gamma_{3c}x), & x\geqq d,\end{cases} \tag{5}$$

where R and T are the reflection and transmission coefficients of the homogeneous slab, respectively, [12]. Real and imaginary parts of all γ-roots are to be taken positively. Realize that E_{hom} for $x\leqq 0$ consists of the incident reconstruction wave and a backward-scattered component. Inside the slab $(0<x<d)$ multiple reflections of the reconstruction wave form a standing-wave pattern.

$G(x,x';z-z')$ is the Green function for the homogeneous slab and it is determined by

$$\left.\begin{aligned}
&(\partial^2/\partial x^2+\partial^2/\partial z^2+k^2n_1^2)G(x,x';z-z')=0, && x\leqq 0,\\
&(\partial^2/\partial x^2+\partial^2/\partial z^2+k^2n_2'^2)G(x,x';z-z')=-\delta(x-x',z-z'), && 0<x<d,\\
&(\partial^2/\partial x^2+\partial^2/\partial z^2+k^2n_3^2)G(x,x';z-z')=0, && x\geqq d,
\end{aligned}\right\}\ 0<x'<d, \tag{6}$$

and the usual continuity requirements across the slab boundaries and the radiation condition as well.

Following the calculation of Maradudin and Mills for the half-space Green's function [10] we start with the Fourier transform of $G(x,x';z-z')$ with respect to $(z-z')$

$$G(x,x';z-z')=1/2\pi \int_{-\infty}^{\infty} g(x,x';\beta)\exp[i\beta(z-z')]\,d\beta \tag{7}$$

and arrive at the following general solution for the resulting system of ordinary differential equations

$$g(x,x';\beta)=\begin{cases} A(x',\beta)\exp(-i\gamma_1 x), & x\leqq 0,\\ i\exp(i\gamma_2|x-x'|)/2\gamma_2+B(x',\beta)\exp(i\gamma_2 x)+C(x',\beta)\exp(-i\gamma_2 x), & 0<x<d,\\ D(x',\beta)\exp(i\gamma_3 x), & x\geqq d, \end{cases} \tag{8}$$

where outside the slab only outgoing waves are assumed. The unknown functions A, B, C, D are to be determined with the help of the continuity conditions: $g(x,x';\beta)$ and $d(g(x,x';\beta))/dx$ to be continuous along $x=0$ and $x=d$. This gives finally

$$g(x,x';\beta)=\begin{cases} -\{\gamma_2\cos[\gamma_2(d-x')]-i\gamma_3\sin[\gamma_2(d-x')]\}\exp(-i\gamma_1 x)/\det, & x\leqq 0,\\ -\{\gamma_2\cos[\gamma_2(d-x')-i\gamma_3\sin[\gamma_2(d-x')]\}*[\gamma_2\cos(\gamma_2 x)-i\gamma_1\sin(\gamma_2 x)]/(2\gamma_2\det), & 0<x<d,\\ -[\gamma_2\cos(\gamma_2 x')-i\gamma_1\sin(\gamma_2 x')]\exp[i\gamma_3(x-d)]/\det, & x\geqq d, \end{cases} \tag{9}$$

$$\det=i\gamma_2(\gamma_1+\gamma_3)\cos(\gamma_2 d)+(\gamma_2^2+\gamma_1\gamma_3)\sin\gamma_2 d,$$

$$\gamma_1=(k^2n_1^2-\beta^2)^{1/2},\quad \gamma_2=(k^2n_2'^2-\beta^2)^{1/2},\quad \gamma_3=(k^2n_3^2-\beta^2)^{1/2},$$

which is valid for $x\leqq x'$ only. To get the appropriate expression for $x\leqq x'$ exchange the primes of x and x'. Notice that $\mathrm{Re}\{\gamma\}\geqq 0$, $\mathrm{Im}\{\gamma\}\geqq 0$. Before solving (3) in the first Born approximation a few comparing remarks concerning the models of Lukosz and Wüthrich [3] and Lee and Streifer [5] are necessary. These models are also based on the first Born approximation. Both approaches formulated with Green's functions yield two different Green's functions, in detail Lukosz and Wüthrich [3] neglected reflections within the slab, which means in our case

$B=C=0$ in (8).

Lee and Streifer [5] preferred the half-space geometry which appears in our approach for

$C=D=0$ in (8).

Consequently, in both papers the reconstruction wave suffers a single reflection at the entry interface of the hologram only. That means, there is no standing wave pattern inside the slab.

Now we start to solve (3). To this end we use (1), (7), (9), and (5). The application of the first Born approximation is generally justified because of the very confined hologram pattern and the small modulation amplitude, see also [3, 5]. To avoid overcoupling between two adjacent DE maxima, they should not lie too close to one another [13].

The approximated scattered field looks like

$$E(x,z)=E_{\mathrm{hom}}(x,z)+E_s(x,z), \tag{10}$$

$$E_s(x,z)=k^2\int_{-\infty}^{\infty}\int_{0}^{d}[\varepsilon(x',z')-n_2'^2]E_{\mathrm{hom}}(x',z')G(x,x';z-z')\,dx'dz' \tag{11}$$

consisting of two conjugated subfields

$$E_s(x,z)=E_{+s}(x,z)+E_{-s}(x,z) \tag{12}$$

which split into a backward-scattered component $(x\leqq 0)$

$$E_{\pm 1s}(x,z)=A_c H/\Phi\left\{\frac{\mu_0 v_0}{\varrho_0}[\exp(i\varrho_0 d)-1]+\frac{\mu_0 v_1}{\varrho_1}[\exp(i\varrho_0 d)-\exp(2i\gamma_{2s}d)]\right.$$
$$\left.+\frac{\mu_1 v_0}{\varrho_2}[\exp(i\varrho_0 d)-\exp(2i\gamma_{2c}d)]+\frac{\mu_1 v_1}{\varrho_3}[\exp(i\varrho_0 d)-\exp(i\varrho_4 d)]\right\}\exp[i(\beta_s z-\gamma_{1s}x)] \tag{13a}$$

and a forward-scattered component ($x \geqq d$)

$$E_{\pm 3s}(x,z) = A_c H/\Phi \left\{ -\frac{\mu_0 \nu_3}{\varrho_0}[\exp(i\varrho_0 d)-1]\exp(i\gamma_{2s}d) + \frac{\mu_0 \nu_2}{\varrho_1}[\exp(i\varrho_5 d)-\exp(i\gamma_{2s}d)] - \frac{\mu_1 \nu_3}{\varrho_2}[\exp(i\varrho_0 d) \right.$$
$$\left. -\exp(2i\gamma_{2c}d)]\exp(i\gamma_{2s}d) + \frac{\mu_1 \nu_2}{\varrho_3}[\exp(i\varrho_5 d)-\exp(i\varrho_6 d)] \right\} \exp[i(\beta_s z + \gamma_{3s}\{x-d\})]. \tag{13b}$$

The following abbreviations were used

$$H = 2\gamma_{1c}k^2 K \Delta(n_2^2), \quad \Phi = \{\mu_0\mu_2 + \mu_1\mu_3[\exp(2i\gamma_{2c}d)]\}[\nu_0\nu_2 + \nu_1\nu_3\exp(2i\gamma_{2s}d)],$$
$$\mu_0 = \gamma_{2c}+\gamma_{3c}, \quad \mu_1 = \gamma_{2c}-\gamma_{3c}, \quad \mu_2 = \gamma_{1c}+\gamma_{2c}, \quad \mu_3 = \gamma_{1c}-\gamma_{2c},$$
$$\nu_0 = \gamma_{2s}+\gamma_{3s}, \quad \nu_1 = \gamma_{2s}-\gamma_{3s}, \quad \nu_2 = \gamma_{1s}+\gamma_{2s}, \quad \nu_3 = \gamma_{1s}-\gamma_{2s},$$
$$\varrho_0 = \pm\gamma_{20} + i\alpha_{2r} + \gamma_{2c} + \gamma_{2s}, \quad \varrho_1 = \pm\gamma_{20} + i\alpha_{2r} + \gamma_{2c} - \gamma_{2s},$$
$$\varrho_2 = \pm\gamma_{20} + i\alpha_{2r} - \gamma_{2c} + \gamma_{2s}, \quad \varrho_3 = \pm\gamma_{20} + i\alpha_{2r} - \gamma_{2c} - \gamma_{2s}, \tag{13c}$$
$$\varrho_4 = 2(\gamma_{2c}+\gamma_{2s}), \quad \varrho_5 = \pm\gamma_{20} + i\alpha_{2r} + \gamma_{2c}, \quad \varrho_6 = 2\gamma_{2c} + \gamma_{2s},$$
$$\gamma_{1s} = (k^2 n_1^2 - \beta_s^2)^{1/2}, \quad \gamma_{2s} = (k^2 n_2'^2 - \beta_s^2)^{1/2}, \quad \gamma_{3s} = (k^2 n_3^2 - \beta_s^2)^{1/2},$$
$$\beta_s = \beta_c \pm (\beta_0 - \beta_r), \quad \gamma_{2c} = (k^2 n_2'^2 - \beta_c^2)^{1/2}, \quad \gamma_{3c} = (k^2 n_3^2 - \beta_c^2)^{1/2}$$

and the $+/-$ signs agree with the corresponding ones in (13a, b).
Take care if $\gamma_{2c}=0$ or $\gamma_{2s}=0$. It is worth mentioning that (13a–c) coincide exactly with (21) of Lee and Streifer [5] after the straightforward simplification $d \to \infty$, $n_2 = n_3$ in (13a).
Finally, the diffraction efficiency is given by

$$\eta_{\pm 1} = \frac{|E_{\pm 1s}|^2 \gamma_{1s}}{|A_c|^2 \gamma_{1c}}, \qquad \eta_{\pm 3} = \frac{|E_{\pm 3s}|^2 \gamma_{3s}}{|A_c|^2 \gamma_{1c}}.$$

backward-scattered field forward-scattered field

2. Numerical Results

In this section several diagrams illustrating the angular selectivity and the thickness dependence of DE are presented and a comparison with [5] is made. The following parameters and assumptions were used throughout the calculations:

- Recording configuration according to Fig. 3.
- Hologram pattern according to (1a) but putting $n_2 = n_2'$.

2.1. Dependence of DE on the Angle θ_c of Incidence of the Reconstruction Wave

Figure 4 exhibits DE of the (+) backscattered wave (solid line) comparing it with the half-space model of Lee and Streifer [5] (broken line). The interference effects due to multiple wave interference are considerable. Also the expected enhancement of the average DE can be clearly seen.
Figure 5 gives a survey of the different DE's that appear in the slab model. With respect to Fig. 4 reduced medium thickness is assumed leading to larger oscillation periods. Quite naturally there are common features with respect to the half-space model:

- the envelope of the oscillating curve, which is mainly determined by the scattering process rather than the slab geometry, coincides qualitatively with the corresponding curves of the half-space model,
- the absolute maxima do appear neither at Bragg incidence nor at the exact relevant critical angeles, where the reconstruction wave or a diffraction order undergoes total reflection. In Fig. 6 this interference-induced shift is considered in more detail.

There two different peak shapes are plotted which belong to different n_3-values. Peak shape deformation and peak location depend on the location of the multiple wave interference peaks for a given slab configuration. Obviously, this effect loses ground with increasing thickness and decreasing refractive index difference between the hologram and the medium behind it. Bragg angle location is also shown in Fig. 6.

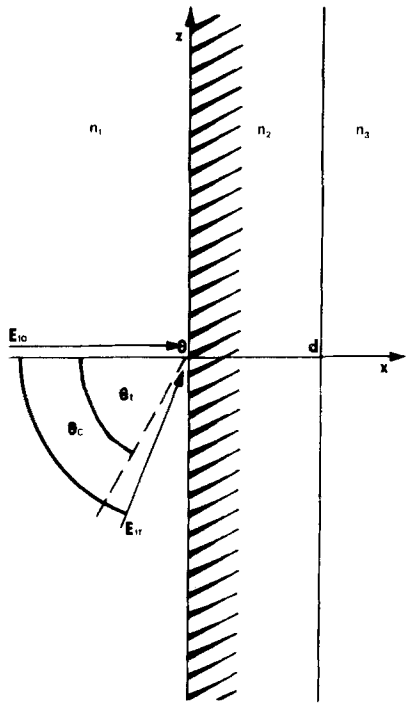

Fig. 3. Recording geometry used for numerical calculations (E_{10}: normally incident object wave; E_{1r}: totally reflected reference wave; $n_1=1.73$; $n_2=n_3=1.58$; critical angle $\theta_t=65.91°$; angle of incidence of the reference wave $\theta_r=67°$; $\lambda=633$ nm)

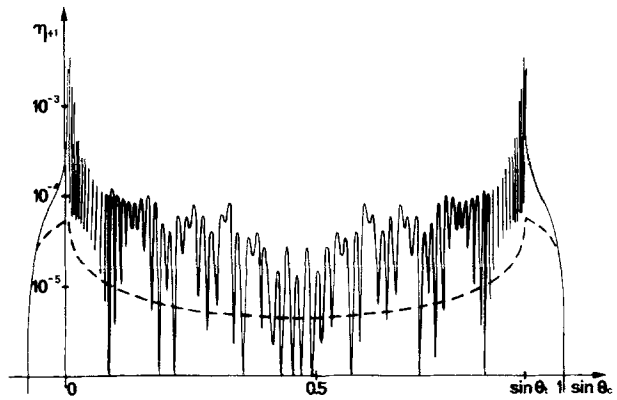

Fig. 4. DE dependence on the angle of incidence θ_c (angular selectivity curves) of the backscattered field (broken line: half-space model; solid line: slab model; $n_3=1.00$; $d=8$ µm; $KA(n_2^2)=0.025$)

2.2. *Dependence of DE on Thickness*

It is well known that the multiple wave interferences in a slab are very sensitive to thickness changes and therefore can seriously affect the experimental results [4].

Figure 7 shows two curves for the backscattered and the transmitted (+) image field, which reveal periodicities of asymmetric shape. Consider each maximum to be followed immediately by a distinct minimum. The periods of the different oscillations are clearly determined by multiple wave interference at the two slab interfaces of the reconstruction wave (long period) and the reconstructed scattered field (short period, appearing in the backscattered field only), respectively. For the present parameter choice both waves mentioned above are homogeneous ones inside the slab, but they travel with different inclinations. Evidently, evanescent waves are affected only within slab thicknesses of the order of the wavelength used. The asymmetric shape of each oscillation reflects the influence of the evanescent grating inside the slab. Particularly, the situation of the interference pattern maxima with respect to the hologram pattern seems to be responsible for the asymmetries.

Let us consider the particular case where the transmitted field is formed by an entirely evanescent scattered field within the hologram (γ_{3s} and γ_{1s} are real but γ_{2s} is an imaginary quantity implying $n_3>n_2$). In this case, there is an energy transfer through an evanescent field region which we call "pseudo optical tunneling".

Figure 8 shows a typical transmitted DE-curve plotted via slab thickness. The oscillations are due to multiple wave interference of the homogeneous reconstruction wave only.

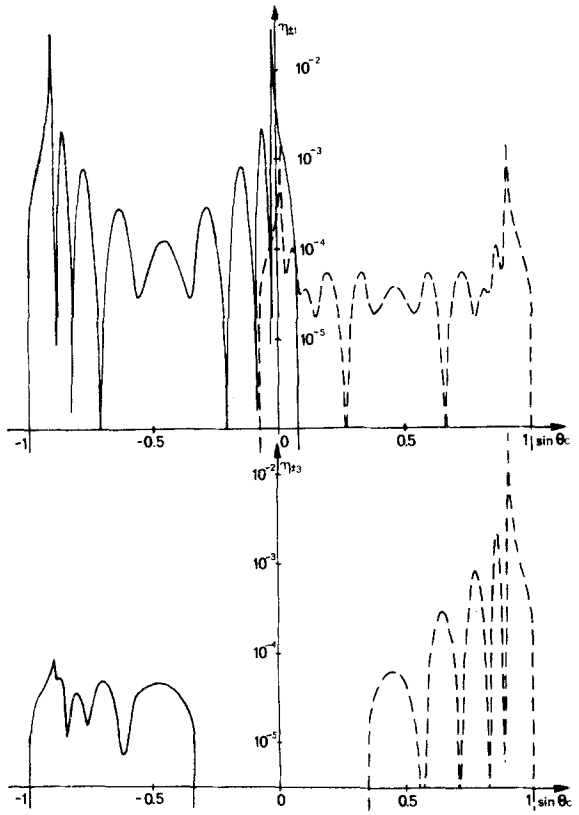

Fig. 5. Angular selectivity curves with respect to all image fields ($\eta_{\pm1}$: backscattered DE; $\eta_{\pm3}$: transmitted DE; broken line: "+" diffraction order; solid line: "−" diffraction order; $d=1$ μm; other parameters like in Fig. 4)

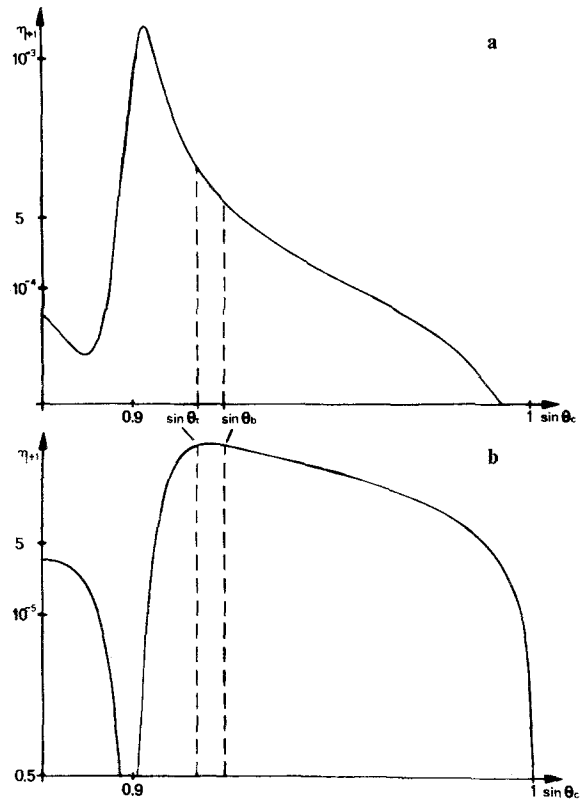

Fig. 6. DE-peak shapes for different surrounding media (a: same hologram like in Fig. 5; b: $n_3^2=3.00$; other parameters unchanged; θ_b: Bragg angle)

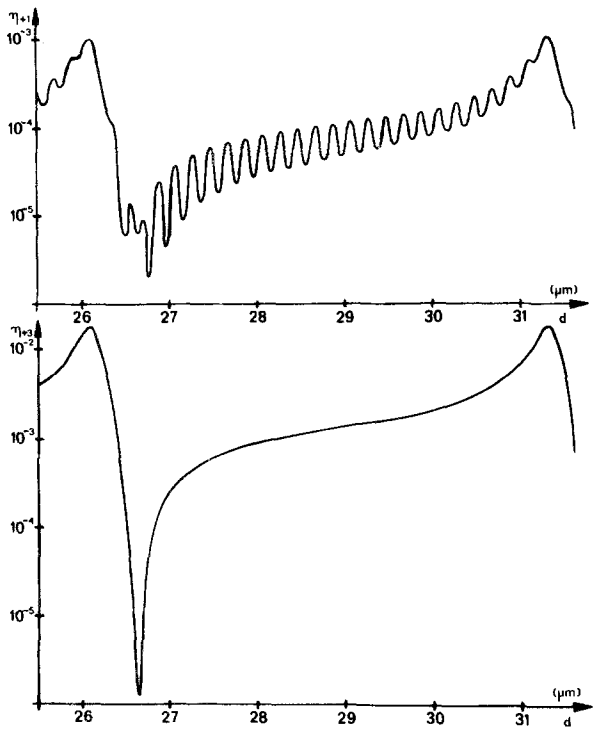

Fig. 7. DE dependence on the slab thickness; backward and forward scattered (+) fields (θ_c: 65.81°; $n_3=1.00$; $K\Delta(n_2^2)=0.008$)

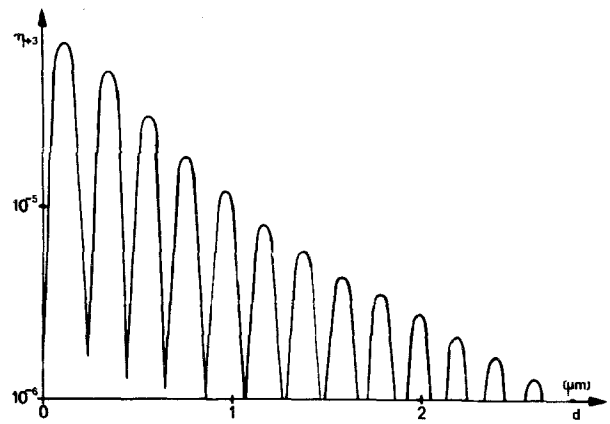

Fig. 8. DE dependence on the slab thickness in the case of pseudo optical tunnelling ($n_3=1.61$; $\theta_c=0.33°$; $K\Delta(n_2^2)=0.025$; $\eta_{\pm3}$: transmitted (+) field diffraction efficiency)

3. Summary

In contrast to previous models [3–6], diffraction efficiencies of evanescent-wave holograms were calculated within the framework of a slab model that takes into account the finite thickness of the recording medium. Using the exact Green's function for a homogeneous slab the scattered (reconstructed) wave were calculated within the first Born approximation of the relevant integral equation for TE polarization.

Multiple wave interferences within the slab lead to characteristic oscillations of the angular selectivity curves and the diffraction efficiency thickness dependence. These oscillations interfere with the intrinsic diffraction effects already predicted by previous models. Multiple reflections give rise to a modified interaction of the inner wave fields with the evanescent hologram grating. This mechanism leads to higher diffraction efficiencies. The shape of the diffraction efficiency maxima appears to be changed and their location slightly shifted away from the relevant angles of total reflection. The effect of pseudo-optical tunneling having no analogue in the half-space configuration is also considered.

It seems to be reasonable to use the presented diffraction efficiency formulas as modified local diffraction efficiency expressions in the model of Lukosz and Wüthrich [7] to calculate "overall-diffraction efficiencies" of waveguide holograms.

References

1. H. Nassenstein: Phys. Lett. **28** A, 249 (1968)
2. O. Bryngdahl: Evanescent wave in optical imaging, in *Progress in Optics*, Vol. XI, ed. by E. Wolf (North-Holland, Amsterdam 1973) pp. 167–221
3. W. Lukosz, A. Wüthrich: Optik **41**, 191 (1974)
4. W. Lukosz, A. Wüthrich: Optik **42**, 315 (1975)
5. W. Lee, W. Streifer: J. Opt. Soc. Am. **68**, 795 (1978)
6. W. Lee, W. Streifer: J. Opt. Soc. Am. **68**, 802 (1978)
7. W. Lukosz, A. Wüthrich: Appl. Phys. **22**, 161 (1980)
8. T. Suhara, H. Nishihara, J. Koyama: 1981 Int. Conf. on Integrated Optics and Optical Fiber Communication, San Francisco, Techn. Digest
9. U. Langbein, F. Lederer: Opt. Acta **27**, 171 (1980)
10. A.A. Maradudin, D.L. Mills: Phys. Rev. B**11**, 1392 (1975)
11. E.G. Williams, J.D. Maynard: Phys. Rev. Lett. **45**, 554 (1980)
12. M. Born, E. Wolf: *Principles of Optics*, (Pergamon Press, London 1959) pp. 322–325
13. S. Sainov, W. Sainov: J. technicheskoy fisiki **44**, 1750 (1979) (in Russian)